Environmental Science Nano

Emerging investigator series: Linking Nanoparticle Infiltration and Stomatal Dynamics for Plant Nanobionics

Journal:	*Environmental Science: Nano*
Manuscript ID	EN-ART-12-2021-001154.R1
Article Type:	Paper

Environmental significance

Fluidic infiltration through the leaf lamina and the displayed stomata pores is a common method by which nanoparticles can be introduced into living plants for applications that include nanoscale sensors and genetic engineering approaches. We develop an automated infiltration platform that enable precise control of the applied pressure and delivery volumes into the leaf mesophyll past the cuticle and the stomata. The developed tool helps to discover novel relationships between stomatal dynamics and nanoparticle infiltration as well as demonstrates promise for optical nanoparticle incorporation into living plants for a variety of emerging applications.

Environmental Science Nano

ARTICLE

Emerging investigator series: Linking Nanoparticle Infiltration and Stomatal Dynamics for Plant Nanobionics

Received 00th January 20xx,
Accepted 00th January 20xx

DOI: 10.1039/x0xx00000x

Volodymyr B. Koman[1], Minkyung Park[1], Tedrick Thomas Salim Lew[1,2,3], Stefan Wan[1], Elliott S. Yarwood[1], Xun Gong[1], Tafsia S. Shikdar[1], Ronald J. Oliver[1], Leslie Jianqiao Cui[1], Pavlo Gordiichuk[1], Rajani Sarojam[4,5], and Michael S. Strano[1,5,*]

Fluidic infiltration through the leaf lamina and the displayed stomata pores is a common method by which nanoparticles can be introduced into living plants for applications that include nanoscale sensors and genetic engineering approaches. The family of techniques that can augment or transform the functions of a living plant using nanoparticles have been labeled *plant nanobionics*. Yet studies of the controlled fluidic infiltration of nanoparticles are currently absent, mainly due to challenges associated with controlling the precision of the process. Herein, we develop an automated infiltration platform for living plants that enables precise control of the applied pressure and delivery volumes into the leaf mesophyll past the cuticle and the stomata. Using three orthogonal measurement techniques of microscopy, gas exchange quantification, and nanoparticle infiltration rates, we study the stomata dynamics and its effect on fluidic infiltration in spinach (*Spinacia oleracea*), cat palm (*Chamaedorea cataractarum*), and peace lily (*Spathiphyllum*) plants. We find that the infiltration efficiency changes throughout the day for spinach plants, while remaining constant for cat palms and peace lily. We conclude that stomata type and open fraction determine the pressure drop and the infiltration efficiency with spinach plants having the most active stomata: the estimated infiltration pressure changes from 115 kPa in the night to 16 kPa in the day due to 70% of stomata reaching the average aperture of 1.0 µm. As an aid to the potential user, we discuss smartphone stomata detection to rapidly characterize leaf surface and smartphone-based nanosensor detection for in-field applications of plant nanobionics. The discovered relationships reported herein and the new tools demonstrated promise optimal and automated incorporation of nanoparticles into living plants for a variety of emerging applications.

Introduction

Plant nanobionics is an emerging intersection of nanotechnology and living plants in the pursuit to create living functional hybrids [1]. The vision encompasses many different applications. By incorporating nanosensors into a living plant, plant nanobionics can transform it into a sensor capable of reporting its own plant physiology and thereby monitor plant health. A new slate of such non-destructive tools can potentially improve agricultural crop yield and growth rate, aiding in the global challenge of food security [2]. Examples to date include: nanosensors for drought [3], arsenic and stress-induced H_2O_2 signaling detection [4], nanoconstructs that boost photosynthesis [5], as well as nanocarriers to deliver genetic cargo to specific organelles [6]. Efforts in plant nanobionics have also focused on producing novel, living devices based on a symbiosis between nanotechnology and plants. Examples include nanotechnology enabled light-emitting plants [7, 8] as well as plants as internet-enabled networks of sensors that can monitor external threats such as explosives [9]. Plants represent an appealing starting platform for these purposes because they continuously grow, self-repair, harvest energy, pump and circulate water, generate their own biofuel and are ultimately carbon negative [5]. Despite these advances, the process of nanomaterial infiltration, being one of the main starting points of plant nanobionic approaches, remains essentially under studied. This work addresses this gap by developing an automated nanoparticle infiltration system that delivers nanomaterials in a controlled and reproducible fashion, linking infiltration and stomatal dynamics in plants.

For nanomaterials to function within the cells and tissues of living plants in plant nanobionic applications, they have to be introduced into the plants past cellular barriers and membranes. Several delivery techniques have been developed in the past decades. Biolistic particle delivery relies on metal particles as carriers to propel infiltration materials into plant cells at high velocities [10]. Although the method is easy to perform, concerns about irreversible cell damage have been raised [11]. Electroporation uses strong electric field pulses to generate transient pores in the cell membrane [12]. Although the

[1] *77 Massachusetts Ave., Department of Chemical Engineering, Massachusetts Institute of Technology, Cambridge, MA, USA*
[2] *Institute of Materials Research and Engineering (IMRE), Agency for Science, Technology and Research (A*STAR), Singapore*
[3] *Department of Chemical and Biomolecular Engineering, National University of Singapore, 4 Engineering Drive 4, Singapore, 117585 Singapore*
[4] *Temasek Life Science Laboratory, National University of Singapore, Singapore, Singapore*
[5] *Disruptive and Sustainable Technologies for Agricultural Precision, Singapore-MIT Alliance for Research and Technology, Singapore, Singapore*
[*] *Corresponding author's email address: strano@mit.edu*
Electronic Supplementary Information (ESI) available, see DOI: 10.1039/x0xx00000x

method is inexpensive and fast, its efficiency is low in plant cells that have a thick cell wall. Agrobacterium-mediated delivery is limited to DNA delivery and relies on the natural ability of *Agrobacterium* to transfer a part of its tumor-inducing DNA into plant cells [13]. This method demonstrates high efficiency, yet it is limited in the host range. Recently, engineered nanomaterial carriers have shown the ability to spontaneously transverse plant cell wall, cell membrane, and even organelle membranes, to deliver cargo into plants. In particular, nanoparticles of gold [14], starch [15], mesoporous silica [16], and carbon nanotubes relying on the theory of lipid exchange envelope penetration (LEEP) [6, 17] have been explored, reaching the ultimate precision of organelle targeted delivery [6]. The method largely addresses the shortcomings of previous approaches by being cheap and facile, applicable to a wide range of plant species including non-model ones, providing the ability to deliver cargo with high efficiency and low toxicity. These advantageous of engineered nanomaterials further elevate the need to understand the process of infiltration, which is central in delivering nanomaterials into plant mesophyll.

There are several modalities of nanomaterial infiltration. Pressurized bath infusion (PBIN) has been proven effective on infiltration of entire plants, but such methods are not practical for larger plants and trees [7]. Spraying technologies are routinely used for fertilizers [18], often employing agricultural spreading agents to lower surface tension and facilitate nanoparticle uptake [19, 20], yet these have limited directionality and uptake, resulting in material waste and contamination of the surroundings. Overall, localized infiltration remains the most widely used technique, allowing for rapid and precise injection of nanomaterials [5]. The technique relies on manual injection using a needleless syringe. The infiltration conditions, such as speed, force, and amount are hardly reproducible. User familiarity with the driving pressure is often required to ensure no leaf damage occurs during the procedure. Further progress in plant nanobionics calls for novel infiltration methods that deliver nanomaterials into plants in a precise and controlled manner.

Microscale pores on a leaf surface, called stomata, dominate plant mechanical resistance during such infiltration, however no studies to date examine stomata effects on infiltration process. Stomata regulate air, water vapor, and gaseous exchange between the environment and plant mesophyll. A pair of guard cells controls stomatal aperture by regulating the cellular hydrostatic pressure in MPa range [21]. Stomatal dynamics is affected by more than 70 different parameters, such as temperature, humidity, light, carbon dioxide, and various plant hormones [22]. Stomatal aperture generally follows diurnal cycle by opening during the day and closing during the night. However, multiple deviations from this pattern have been reported. For instance, Smith *et al.* observed spatially and temporally non-uniform stomatal dynamics in *Commelina communis* leaves [23]. Laisk *et al.* identified that stomatal aperture follows either normal or bimodal distributions in *Vicia faba*, *Hordeum vulgare* and the *Spannungsphase* plants [24]. Terashima *et al.* observed patchy areas of open and closed stomata in *Helianthus annuus* and *Vicia faba* leaves [25]. Mott *et al.* identified hydraulic coupling mechanism between neighboring stomata in *Xanthium strumarium* plants [26]. It is not clear whether these effects of stomatal dynamics will translate into the hydrodynamic resistance and, if so, to what extent.

Here, we establish the first link between stomatal activity and infiltration efficiency using a novel system for automated infiltration. The system ensures controlled infiltration force, duration, and amount. Microscopic images and gaseous measurements reveal different portions of active stomata across three plant species. Stomatal activity is directly correlated with the infiltration efficiency as it is shown to form the dominant hydrodynamic resistance for the infiltration. Furthermore, the presence of trichomes can prohibit infiltration as revealed among a number of species tested by a stomameter, a hand-held microscope for rapid leaf assessment. The infiltration process is shown to affect plant's CO_2 assimilation capabilities that are restored after 7 days. Finally, we demonstrate smartphone-based nanosensor detection to complete a suite of portable techniques for interfacing and observations of nanomaterials interfacing living plants. The optimized conditions and methods will advance fluidic infiltration, aiding the development of next-generation sensing and genetic engineering applications in plants and food that improve crop yield and growth rate, as well as minimize the environmental impact.

Results and discussion

Nanoparticle Infiltration Effects

The infiltration procedure needs to overcome the leaf lamina hydrodynamic resistance, while operating below the leaf threshold damage. For the manual infiltration, this requirement translates into the following operator's actions: a syringe is gently applied to a leaf lamina with one hand, while a finger of another hand provides a soft back support for a leaf. The shortcoming of such approach is reproducibility in terms of applied pressure as well as infiltrated volume. To study infiltration effects in a reproducible manner, we develop an automated infiltration system where a leaf is sandwiched between a newton force meter and a syringe (**Fig. 1a,b**). A microfluidic pump allows programming the desired infiltration speed and duration to obtain similar volumes across multiple experiments. The newton force meter sustains a constant pressure applied on a leaf (**Fig. 1d**). The system enables highly controlled infiltrations like in **Fig. 1c**, where infiltrated nanomaterials spread through leaf mesophyll only to be confined by major leaf veins.

An important consideration for the system is the ability to achieve a tight seal between a syringe and a non-planar leaf without damaging the latter. To this end, a soft support layer needs to be added behind a leaf that will deform under the applied pressure, helping to planarize the leaf surface. To evaluate the properties of the support layer that favor infiltration, we consider the following force balance. The force (F) applied by a syringe and the respective pressure (p) spread

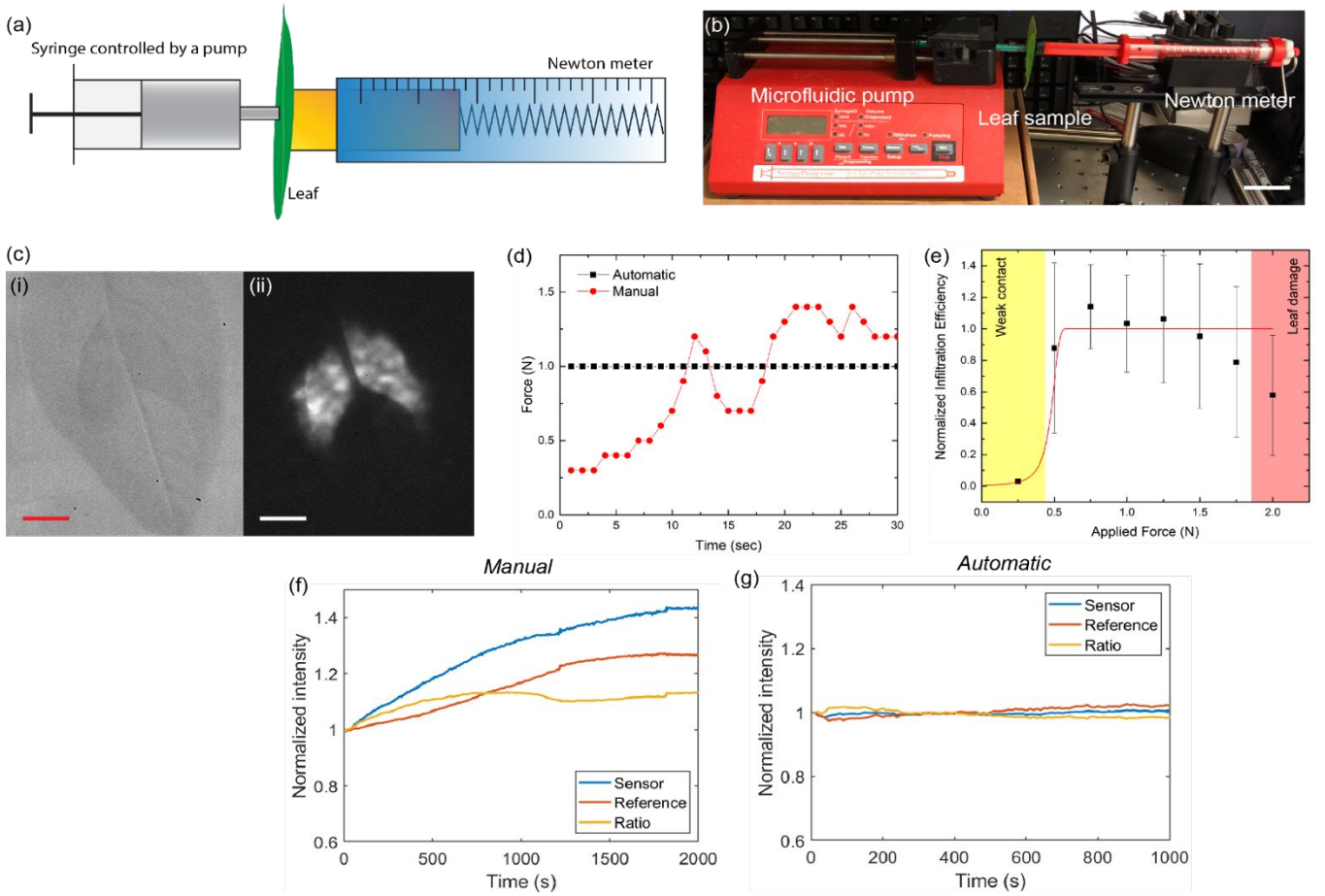

Fig. 1. Automated nanoparticle infiltration. A schematic (a) and the experimental set-up (b) of the automated infiltration system. Scale bar is 1 cm. (c) A bright-field image (i) and a near-infrared fluorescent image (ii) taken after infiltrating a spinach leaf with sensors (10 mg/l GT_{15}-carbon nanotube) at 100 µl/min flow rate with 1 N applied force for 30 sec duration. Scale bars are 1 cm. (d) A comparison of applied force between manual and automatic infiltrations. (e) Normalized infiltration efficiency defined as the cumulative sensor (10 mg/l GT_{15}-carbon nanotubes) intensity for 3-weeks old spinach infiltrated at 1 PM local time (n=5) at 100 µl/min flow rate with 1 N applied force for 30 sec duration. The red line represents a fit described in the text. Normalized near-infrared fluorescent intensity of two carbon nanotube solutions marked as 'sensor' (10 mg/l GT_{15}-carbon nanotubes) and 'reference' (10 mg/l C_{30}-carbon nanotubes) as well as their ratio infiltrated at t=0 using manual (f) and automatic system at 100 µl/min flow rate with 1 N applied force for 30 sec duration (g) in 3-weeks old spinach.

over the syringe tip area (A_s) compresses a leaf (Δx_{leaf}) and a support behind it (Δx_{sup}) (**Fig. S1**):

$$F = pA_s = k_{leaf}\Delta x_{leaf} = k_{sup}\Delta x_{sup}, \quad (1)$$

where k_{leaf} and k_{sup} are spring constants of the leaf and the support, respectively. If the support material is harder than the leaf ($k_{sup} > k_{leaf}$), then the leaf compression will dominate ($\Delta x_{leaf} > \Delta x_{sup}$), leading to early damage. On the other hand, if the support is too soft ($k_{sup} \ll k_{leaf}$), then its compression will be large, promoting leaf bending that necessarily impedes infiltration (**Fig. S2**). To satisfy both of these conditions, we employed a polyethylene foam with 1 MPa Young's modulus and estimated $3 \cdot 10^4$ N/m spring constant (using 1 cm^2 area and 3 mm thickness). This is a few times lower than the respective values of a leaf 10 MPa Young's modulus [27] and estimated $1.9 \cdot 10^5$ N/m spring constant (using A_s = 5.56 mm^2 tip syringe area and 0.3 mm thickness).

To evaluate the infiltration efficiency, we used a model fluorescent probe in the form of near-infrared carbon nanotube sensors [4]. The infiltration efficiency was defined as the cumulative fluorescence intensity measured by standoff imaging, which corresponds to the total volume of the infiltrated solution, while the spatial spreading is defined by the mesophyll structure (**see Methods**). To compare manual and automated techniques, we monitored temporal intensity traces post-infiltration in 3-weeks old spinach (*Spinacia oleracea*) leaves. To account for any possible leaf movement, every method was applied to a leaf lamina on both sides of a midvein. While manual infiltration was associated with a 30-min stabilization period needed to circumvent up to 40% intensity drift (**Fig. 1f**) due to the possible residual probe movement post-infiltration, the automated infiltration resulted in a stable temporal trace immediately after the infiltration with <3% intensity drift (**Fig. 1g**). The method works seamlessly, allowing to rapidly and controllably infiltrate plants, optimizing various infiltration conditions. Upon studying different applied forces, we found a range of 1.0 to 1.5 N to yield optimal infiltration efficiency for spinach leaves (**Fig. 1e, Table S1**). At F <0.5 N, a contact between a syringe and a leaf is not tight due to the non-planar leaf nature, causing leaks. Under a given flow rate (Q), the fluid pressure drop in the syringe is divided between two channels: leaf non-uniformities with hydrodynamic resistance R_1 and stomatal pores with R_2. The infiltration flow rate, Q_2, can hence be found as:

$$Q_2 = \frac{Q}{1 + R_2/R_1}. \quad (2)$$

The hydrodynamic resistance R_1 is determined by the leaf gap height (h) that, in turn, decreases with applied force, following Hooke's law:

$$R_1 = \frac{A}{h^3} = \frac{A}{(h_0 - F/k_{sup})^3}, \quad (3)$$

where A is the proportionality constant determined by fluid viscosity, gap width and length, h_0 is the initial size of leaf gap, typically ranging from 1 to 30 μm [3]. At F>0.5 N, the contact between a syringe and a leaf is well established with $Q_2 = Q$, leading to efficient nanosensor infiltration. At F>1.5 N, we observed the decrease in the infiltration efficiency due to the leaf compression and bending, eventually leading to the leaf damage.

Infiltration Efficiency Correlated with Stomatal Dynamics

To study the effect of stomata on the infiltration efficiency, we have used automated infiltration system on spinach plants, cat palms (*Chamaedorea cataractarum*) and peace lily (*Spathiphyllum*) during different times of the day. For cat palm and peace lily, the infiltration efficiency does not statistically differ between three infiltration times throughout the day. In contrast, spinach plants demonstrate higher infiltration efficiency at 1 PM local time as compared to infiltrations at the beginning (7 AM) and the end (7 PM) of the day (**Fig. 2a,g,m**). To further understand stomatal dynamics in these species, we employed two complementary techniques: (1) optical microscopy and (2) gas exchange measurements. Optical microscopy micrographs showed that there are two distinct populations of stomata apertures for cat palms: closed stomata and stomata with the average aperture of 0.6 μm (**Fig. 2b,c**), but these populations do not change between day and night (**Fig. 2d,e**). Peace lily (**Fig. 2h,i**) demonstrated partial stomatal dynamics with around 35% of stomatal opening during the day (**Fig. 2g,k**). Spinach plants (**Fig. 2n,o**) showed higher stomatal dynamics with nearly 70% of stomata opening during the day as compared to the night (**Fig. 2p,q**). Stomatal conductance measurements, that correlate with leaf evaporation rates, show very low values for cat palm (**Fig. 2f**), around 40% modulation between day and night for peace lily (**Fig. 2l**), and 70% modulation for spinach (**Fig. 2r**). The differences in stomatal dynamics between plant species may be related to the variation in environmental conditions that the plants are adapted to thrive in [28].

Using stomatal information, we further calculate the pressure necessary for successful infiltration, correlating it with the observed infiltration efficiencies. The infiltration efficiency is determined by the hydrodynamic resistance of the leaf, which is composed of stomata and mesophyll. Approximating stomatal aperture as a rectangular channel with width w, height h, and length l, the pressure drop can thus be found as:

$$\Delta P = RQ = \frac{12\mu L}{wh^3}Q, \quad (4)$$

where μ is water viscosity (10^{-3} Ns/m^2). The solution viscosity depends on the nanoparticle volume fraction, but here we assume that the solution is in the infinite dilute limit. The imposed infiltration pressure promotes further stomata opening by acting on the guard cells [21]. This effect can be taken into account using an empirical relationship between stomatal pore width and the guard cell hydrostatic pressure as described by Franks *et al.* [21]:

$$\frac{w}{w_{max}} = \alpha - \beta e^{-\frac{P}{\gamma}}, \quad (5)$$

where α, β, and γ are empirical values equal to 1, 0.848, and 1.23×10^6 Pa, respectively. The adjusted width values are used to estimate the minimum infiltration pressure (**Table 1**). In particular, the pressure needed to infiltrate spinach plants in the night (115 kPa) is found to be 7 times higher compared to the one during the day time (16 kPa), correlating well with the observed difference in infiltration efficiencies. Closed stomata are associated with high hydrodynamic resistance that requires higher pressure to sustain the flow rate, increasing leak probability as the fluid pressure exceeds the sealing pressure. In contrast, the difference in the infiltration pressures for cat palm and peace lily in the day and night is less than 200%. The infiltration force of 1 N was used as an optimal value found in **Fig. 1**. Estimating the syringe area of 5.56 mm^2, we obtain the contact pressure of 180 kPa, which is above the pressure drop across stomata, confirming that these plants can be infiltrated without tissue damage. The pressure drop in the leaf mesophyll corresponds to only 0.7 Pa, which can be overcome by capillary force due to infiltration (100 Pa), estimated from the mesophyll length of 1 cm, width of 1 cm, and height of 3 mm [7].

Table 1. Stomatal characteristics and estimated pressure drops necessary for infiltration at 100 μl/min flow rate calculated as described in the text. Stomatal width and aperture were extracted from microscopy images, while stomatal height – from confocal images in [29].

	Cat Palm	**Peace Lily**	**Spinach**
Depth (μm)	5	5	5
Width (μm)	10	20	10
Fraction of open during the day	0.3	0.35	0.7
Open aperture (μm)	0.6	1.3	1.0
Fraction of open during the night	0.24	0	0
Open aperture (μm)	0.67	N/A	N/A
Day pressure drop (kPa)	**77**	**16**	**16**
Night pressure drop (kPa)	**68**	**26**	**115**

Environmental Science Nano

ARTICLE

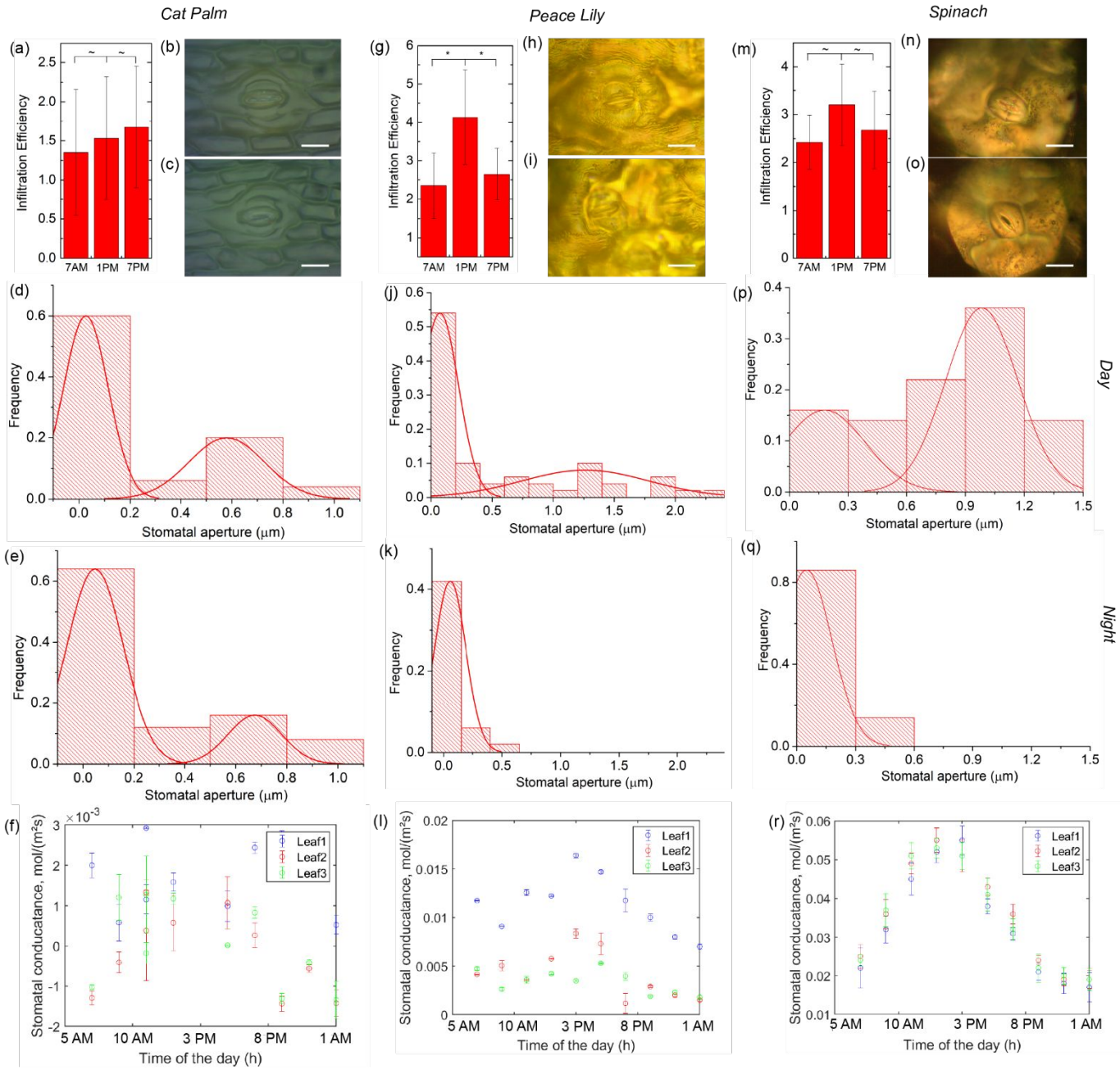

Fig. 2. Correlating stomatal dynamics and infiltration efficiency. (a) Infiltration efficiency (10 mg/l GT_{15}-carbon nanotubes) for a cat palm performed at various local times (n=5) at 100 μl/min flow rate with 1 N applied force for 30 sec duration. Representative micrographs of closed (b) and open (c) stoma. Scale bars are 10 μm. The frequency of stomatal apertures measured at 1 PM, marked as day (d), and at 7 PM, marked as night (e). At least 100 stomatal pictures were used for every histogram. Histogram size bin is determined by the diffraction limit as a measurement error. (f) Stomatal conductance for three leaves on a cat palm (n=3). Same as (a–f) for a peace lily (g–l) and a spinach (m–r). Gaussian distribution was fitted with the solid lines to represent different stomata sub-populations. The tilde (~) denotes statistically insignificant results, while the asterisk (*) – statistically significant.

Hand-held Stomameter for Rapid Stomatal Assessment

Besides stomatal dynamics, leaf morphology often becomes a limiting factor during the infiltration process due to the presence of veins or trichomes [3]. The ability to rapidly inspect leaf surface is, therefore, critical. This is especially true in the field environment, where a microscope might be absent. Additionally, the ability to assess stomatal density would bring

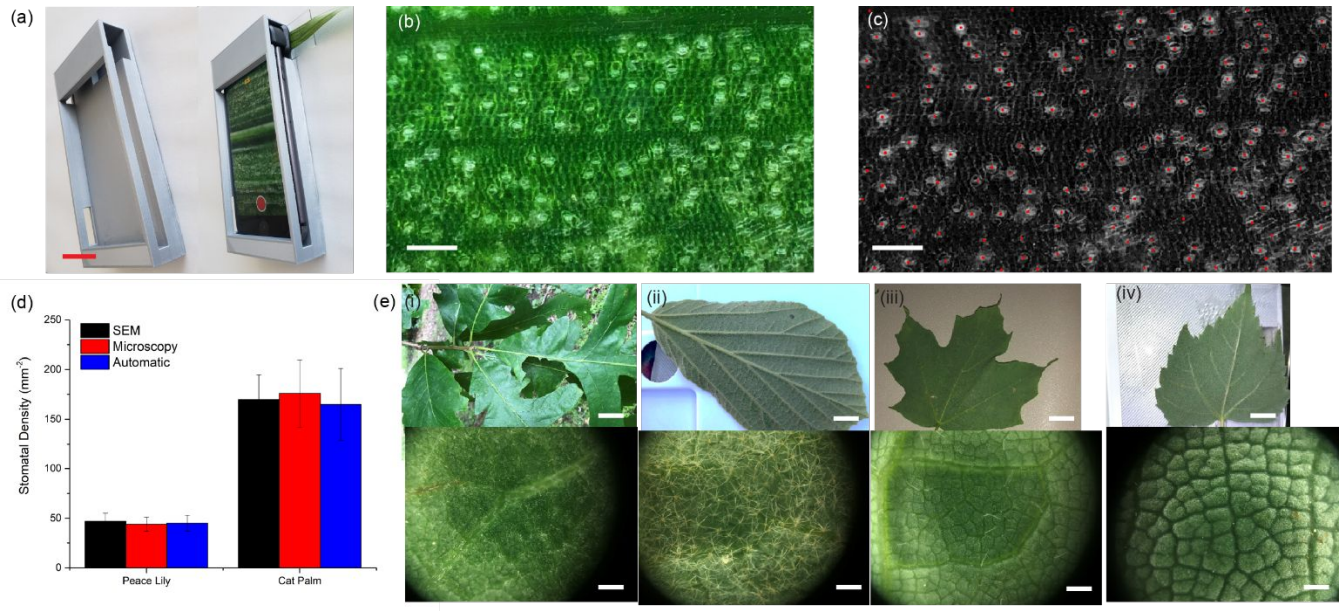

Fig. 3. Rapid assessment of stomata by a hand-held stomameter. (a) A stomameter, a smartphone-based stomatal microscope: (left) 3D-printed case, (right) assembled device clamping a cat palm leaf. Scale bar is 1.5 cm. (b) A picture of peace lily stomata. Scale bar is 100 µm. (c) Rapid stomatal counting by a home-built thresholding algorithm, where red points correspond to identified stomata. (d) Stomatal density comparison as assessed by SEM, optical microscopy, and stomameter. (e) Leaf structures assessed by a stomameter for various plant species in Harvard Arboretum: (i) Burr oak (*Quercus macrocarpa*), (ii) 'Arnold Promise' (*Hamamelis×intermedia*), (iii) Sugar maple (*Acer saccharum*), (iv) Tiliaceae (*Tilia mongolica*). Scale bars are 1 cm for top images and 100 µm – for bottom ones.

additional information about a plant's state. Indeed, environmental factors, such as carbon dioxide, water and nutrient availability, illumination, and temperature, may all affect stomatal density [30]. Here, we have developed a hand-held device, called stomameter, which is a portable instrument to capture microscopic leaf surface images and rapidly analyse stomatal features and density. The device is composed of a smartphone with off-the-shelf microlens assembled in a home-built 3D printed case to allow for precise leaf positioning and focusing (**Fig. 3a**). Stomameter allows stomatal imaging with 3 µm resolution (**Fig. 3b**) with the future improvements in optics and software targeted to resolve stoma open/close states. The instrument is coupled with a custom-built image recognition software to rapidly count stomata (**Fig. 3c**), achieving the average recognition precision of 97%. The counting algorithm relies on several digital filters (noise removal, frequency-based filtering, and adaptive thresholding) interfaced with a set of user-controlled parameters. The software relies on specific stomatal features that are identified and set by a user, allowing for rapid counting without the need of a large training set typically used by neural networks [31]. The extracted values of stomatal density are in excellent agreement with manual stomatal counting from both SEM and microscopy images (**Fig. 3d**). Stomameter was field tested on 18 wild species at Arnold Arboretum of Harvard University in Boston. A number of species were identified to contain trichomes that impede infiltration process by obstructing a tight seal between a syringe and a leaf (**Fig. 3e**), demonstrating stomameter potential to rapidly inform users on the possibility of infiltration. Future efforts will include trichome classification according to their size and shape with the stomameter ability to estimate the pressure for optimal infiltration

Long-Term Effects of Plant Nanobionics

To understand long-term effects of infiltration, we have monitored leaf assimilation capabilities that are related to efficiency of photosynthetic machinery and carbon fixation properties. Infiltration with either water or nanomaterial lowered the assimilation of peace lily leaves right after the infiltration as compared to control taken one day before (**Fig. 4a,b**). The presence of water in the mesophyll offsets the water balance of adjacent cells and increases the mesophyll thickness, affecting the absorption of incoming light. Leaves infiltrated with water returned to the pre-infiltrated state within 3 days post infiltration (**Fig. 4c, Table S2**), indicative of a recovery process to evaporate infiltrated water and to stabilize biochemical process skewed by the excess of water. Leaves infiltrated with carbon nanotubes returned to the pre-infiltrated state only after 7 days (**Fig. 4d**). The engineered wrapping renders the infiltrated nanotubes to spontaneously traverse cellular and chloroplast membranes [4, 32]. These nanoparticles were also previously shown to bind to chloroplast thylakoid membranes and stroma, briefly augmenting photosynthetic activity before decreasing it due to the induced reactive oxygen species generation [5]. Naturally, the original nanotube wrapping is displaced with biological proteins over time, disrupting the nanotube functionality [33]. Our control experiments of infiltrating only buffer showed similar trends as nanotube solutions (**Fig. S3**), indicating that buffer pH was responsible for the delayed recovery. These results are in agreement with previous works that demonstrated no impact on leaf chlorophyll content after carbon nanotube infiltration over 20 days period [5, 9].

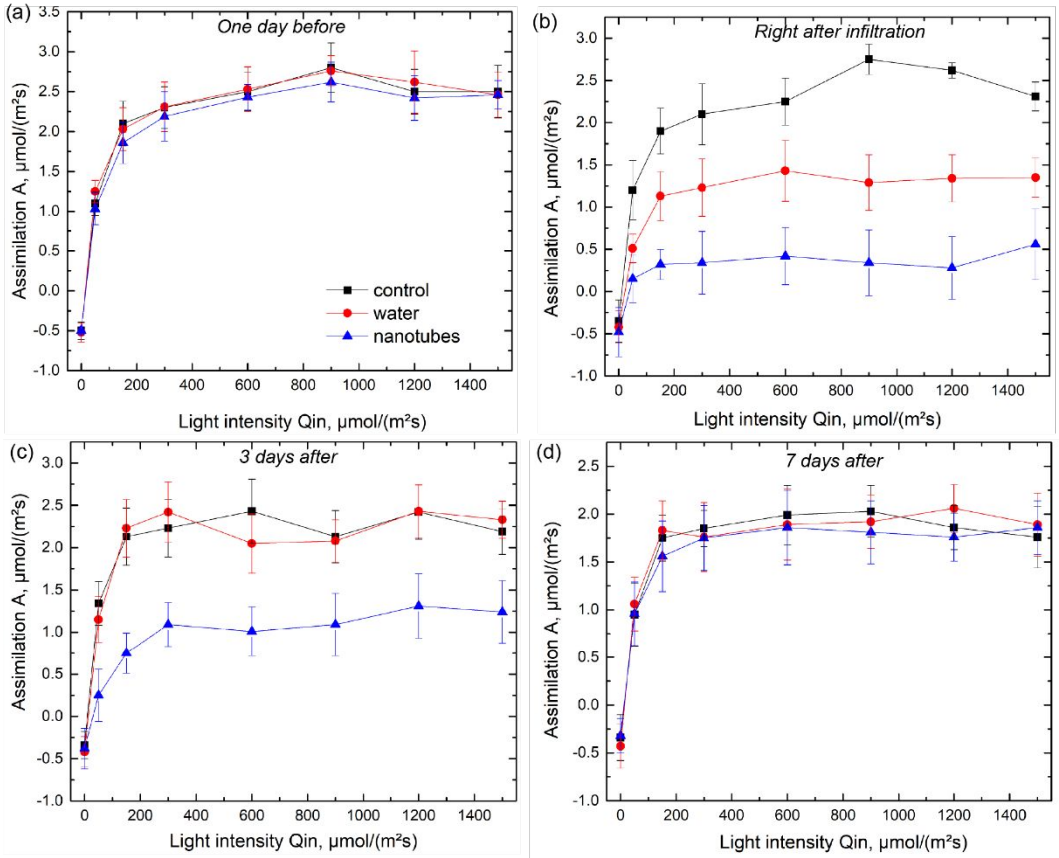

Fig. 4. Effects of material infiltration. Leaf assimilation of Peace Lily plants one day before infiltration (a), right after infiltration (b), three days after (c), and seven days after (d). Measurements were taken around 12-2 PM local time. Plants were infiltrated with water and 10mg/l GT_{15} carbon nanotubes in buffer (n=3).

Automating Plant Nanobionics with Handheld Technology

One application of plant nanobionics aims to interface plants with optical nanosensors. The latter aid in studying plant biochemical reactions [4] as well as transform plants into self-powered pre-concentrators and autosamplers [9]. Optical nanosensors bring the advantage of wireless readout at standoff distances and extraordinary multiplexing capabilities, not being confounded by necessity of wiring. Furthermore, we have recently developed a mathematical framework, called Lipid Exchange Envelop Penetration (LEEP), to engineer nanomaterials that spontaneously traverse cellular and organelle membranes [32, 34]. LEEP allows developing nanosensors interfaced with specific cellular compartments. To translate these advances to agricultural applications, we developed a low-cost fluorescent system based on a commercial smartphone (**Fig. 5a**). A flashlight and a low-cost laser were employed as excitation sources. As a proof of concept, we performed *in vitro* calibration of GT_5 carbon nanotubes conjugated with a TOPRO1 (TP) dye that emits at 540 nm. This complex has been demonstrated to be selective to As^{3+} solution [35]. The intensity quenching response was found to be dependent on the excitation source, as investigated with laser power of 10 mW/cm² vs. the flashlight power of 1 mW/cm² (**Fig. 5b**). This portable system enabled non-destructive imaging of infiltrated fluorescent nanosensors *in planta* (**Fig. 5c,d**).

Encouraged by the *in vitro* results, we investigated if the portable detection system can be applied *in planta*. Elevated levels of arsenic metalloids are often present in groundwater, posing serious risks to food safety, human nutrition and plant health [36, 37]. Monitoring the uptake of arsenic within living plants is therefore important to develop strategies to mitigate arsenic contamination in our food chain. A plant nanobionic sensor, composed of living plants interfaced with engineered nanosensors selective to arsenite, was recently introduced for sensitive detection of arsenic from the belowground environment autosampled by the plant's extensive root system. Using TP-GT_5-SWNTs as a sensor, nanosensors embedded in a spinach quenched by 45% upon the introduction of 10 µM arsenic metal in the vicinity of a detached leaf at the petiole (**Fig. 5e**). This demonstrates the capability of detecting arsenic using a portable system for in-field applications.

Nanosensors also allow to monitor plant health and physiological processes. As sessile organisms, plants rely on complex signaling mechanisms using rapid cell-to-cell communication by H_2O_2 and Ca^{2+} pathways to register biotic and abiotic stresses [38]. We have recently found that H_2O_2 concentration profile induced by mechanical wounding follows a logistic waveform [4]. Remarkably, this waveform encodes the plant native capacity to scavenge H_2O_2, as represented by the parameter α which also affects the symmetry of the logistic waveform. We infiltrated spinach plants with ssGT_{15}-wrapped carbon nanotubes to act as near-infrared fluorescent sensors for H_2O_2 *in planta*. The nanosensor intensity quenches upon

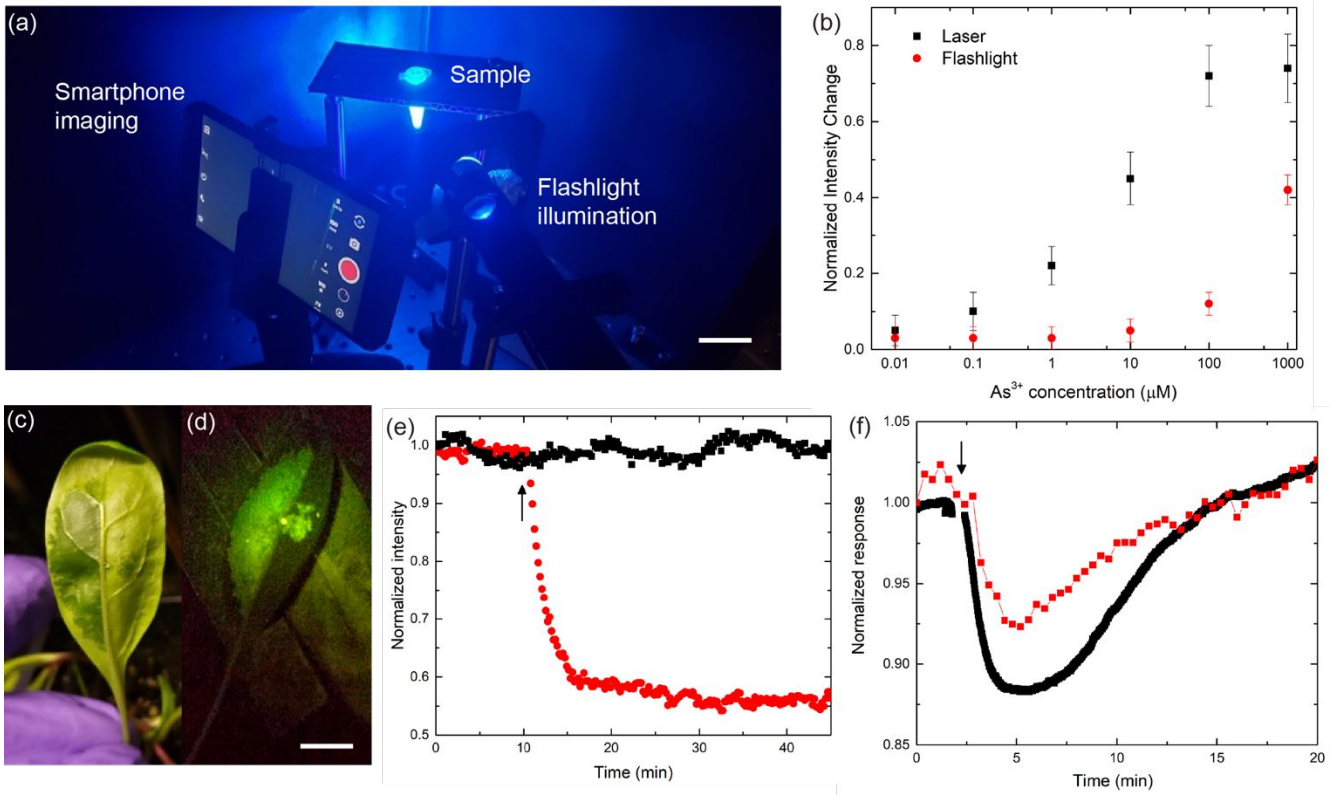

Fig. 5. Low-cost standoff imaging system based on a smartphone. (a) An experimental layout for smartphone-based fluorescent imaging equipped with fluorescent filters as described in the text. (b) In vitro calibration curve for detecting As3+ using carbon nanotube-TO-PRO (10 mg/l) dye excited with two different light sources. A standoff bright-field (c) and fluorescent (d) image taken by a smartphone for TP-GT5-wrapped carbon nanotubes (10 mg/l) infiltrated into a spinach leaf. (e) Detecting As3+ with TP-GT5-wrapped carbon nanotubes after the addition of 10 μM As3+ in the vicinity of a detached spinach leaf at the petiole (red) and a control with buffer addition (black). A black arrow indicates the addition time. (f) Detecting plant wounding in spinach plants with 10 mg/l GT15-wrapped carbon nanotubes as nanosensors using InGaAs camera (black) and Raspberry Pi camera (red). A black arrow represents the time point of wounding. Scale bars are 1 cm.

H_2O_2 addition and restores to its initial level, showing reversible behavior, upon H_2O_2 decomposition [4]. The mechanical wounding of a leaf tip induces H_2O_2 signaling response with the infiltrated sensor demonstrating a quenching response followed by a restoration dynamics after several minutes (**Fig. 5f**). This response was captured by a dual detection platform: a portable and low-cost Raspberry Pi camera and a liquid nitrogen-cooled InGaAs camera. Although Pi camera showed markedly weaker response as compared to InGaAs camera, due to the limited spectral range of its Si detector, the extracted values of α, 0.20±0.04 for Pi camera vs. 0.19±0.03 for InGaAs camera, are in excellent agreement. This demonstrates the ability of nanosensors to tap into previously unknown plant physiological responses and highlights the validity of using low-cost electronics to intercept such signals. Although our results indicate changes in leaf assimilation, previous work demonstrates that nanosensor infiltration has no effect on leaf signalling [4].

Conclusions

We have found that infiltration efficiency varies with the applied force between a syringe and a leaf, with the maximum at 0.7 N. Analytical model shows that this force is necessary to secure a tight seal with a non-planar leaf. Higher infiltration efficiency is also associated with bigger stomatal openings as these introduce the dominant hydrodynamic resistance. As such, infiltration efficiency changes throughout the day for plant species with active stoma, such as spinach. The developed stomameter allowed us to identify a number of species with trichomes that impede leaf infiltration as well as to rapidly count number of stomata. We further utilized plant nanobionics approach to demonstrate how plants interfaced with optical nanosensors can act as self-powered preconcentrators for arsenic detection in groundwater. Nanosensors can also be used for monitoring H_2O_2 signaling induced by mechanical wounding where we demonstrated that the ability to extract plant's H_2O_2 scavenging capacity and demonstrated the validity to use low-cost cameras. The infiltrated plants were shown to return to their original state within 7 days after infiltration. These results demonstrate the augmentation of plant nanobionic approach with controlled nanoparticle delivery and portable imaging system to impact agriculture applications targeted to enhance crop yield and growth rate. Importantly, the developed methods and the optimized conditions increase the precision of nanobionic delivery while minimizing waste and any potential disturbances on the surrounding environment.

Methods

Plant material. Seeds of carmel spinach (*S. oleracea*) were purchased from David's Garden Seeds. Plant seeds were grown Fafard Professional all-purpose blend potting soil in a six-cell seedling tray, with each tray measuring 2.5x2.5x3 in^3. Spinach plants were grown for three weeks before experimental use. Peace lily (*Spathiphyllum wallisii*) plants, approximately 25 cm-tall, were purchased from a local supermarket planted in a pot of 13 cm in diameter and 15 cm in height. Cat palms (*Chamaedorea cataractarum*), 3-foot tall, planted into 25-inch grower's pot were purchased from Costa Farms. For controlled growth environment, plants were grown in a Conviron Adaptis 1000 growth chamber with 12-h-light/12-h-dark photoperiod at 50 µmol/(s·m^2), 60% relative humidity, and day and night temperatures of 25ºC and 18ºC respectively.

Preparation of nanosensors. Raw HiPCO SWNTs were purchased from NanoIntegris (lot HR27-104). All DNA oligonucleotides were purchased from Integrated DNA Technologies. One mg of DNA and 0.25 mg of HiPCO SWNT were mixed in 1 ml of 50 mM NaCl. The mixture was sonicated with 3 mm probe tip for 20 min at 40% amplitude in an ice bath. The sample was then centrifuged twice at 16,000 g for 90 min each to remove unsuspended SWNT bundles that precipitate into a pellet. The concentration of the SWNT suspension was determined using its absorbance at 632 nm and extinction coefficient of 0.036 mg/(L·cm). TOPRO1 dye was purchased from ThermoFisher, catalog #T3602. TP-$(GT)_5$-SWNT preparation followed in distinct proportions, while all subsequent steps remained the same: 1 mg of SWNT was mixed with 0.25 mg of DNA and TP solution at a dye: DNA ratio of 1:4 in 1 mL of deionized water.

Infiltration system. The infiltration of materials was performed using a needless 1 ml syringe to the abaxial side of the leaf. For the automatic infiltration, a syringe was fixed onto a pump (NE-1000, New Era). An intact leaf was secured on a 3 mm-thick polyethylene foam using a double-side tape and sandwiched between a needless syringe and a newton force meter (Ajax Scientific). A typical infiltration process was performed at 100 µl/min flow rate with 1 N applied force for 30 sec duration. The abaxial side of the leaf was then briefly washed with water to remove excess materials on the leaf surface.

Microscope imaging. Optical stomatal aperture measurements were performed using an inverted microscope Zeiss Observer Z1. Short exposure (typically 20 ms) pictures were taken to minimize illumination effect on a stoma sate. Electron imaging was performed by a tungsten source SEM (6010LA, Jeol), typically at 20kV, after sputtering of 20 nm carbon to protect against static charges.

Gas exchange measurements. Stomatal conductance and assimilation measurements were performed using LI-Cor 6800. The chamber flow was set to 500 µmol/sec with overpressure of 0.1 kPa. The humidity was kept 60%, CO_2 level at 400 µmol/mol, and fan speed at 10000 rpm. The air temperature and light were matched to that of the growth chamber at the time of the measurement.

Stomameter. The Stomameter was built using 3D printed enclosure produced using Ultimaker 3 3D printer. The enclosure contains a smartphone (Iphone 8, Apple) and a lens (Micro 400X, Nurugo) for imaging. The recognition algorithm was programmed using Matlab R2019a.

Stand-off imaging. The imaging was performed in the fluorescence mode with an excitation source and an imaging device both being ~10-15 cm away from a plant specimen. For near-infrared sensing, a 785 nm laser (Invictus, Kaiser Optical Systems) with an incident power of 15 mW was used as the excitation source. A short-pass filter (FELH 900 nm, Thorlabs) was placed in front a detector, either InGaAs detector (OMA V, Princeton Instruments) paired with a magnifying lens (AF Micro-Nikkor 60 mm f/2.8D, Nikon) or CCD detector (f=3.6 mm 1/2.7'', Raspberry Pi). Typical integration times were 1 s for InGaAs detector and 5 s for CCD detector with images being corrected against background and dark current noise. For visible sensing, either a laser (MDL-III-520L, OptoEngine) or a flashlight (Cree XP-L LED 1050 Lumens, Soonfire) with 530 nm short pass filter were used as excitation sources. A smartphone (Iphone 8, Apple) equipped with 530 nm long-pass filter was used for imaging. Wound was inflicted using a sharp-tip forcep across the midrib near the leaf tip 1 cm away from the sensor spots. The arsenic detection was performed by introducing As^{3+} solution near the root system.

Data availability. All raw and processed data generated in this work, including the representative images provided in the manuscript, are available from the corresponding authors upon reasonable request.

Conflicts of interest

The authors declare no conflict of interest.

Acknowledgements

V.B.K. was supported by The Swiss National Science Foundation (projects no. P2ELP3_162149 and P300P2_174469). T.T.S.L. was supported on a graduate fellowship by the Agency of Science, Research and Technology, Singapore. M. P. is grateful for the support of the Samsung Scholarship. The sensing aspect of this work was supported by the USDA National Institute of Food and Agriculture, project 2021-67021-33999. The translational development was supported in part by the National Research Foundation (NRF), Prime Minister's Office, Singapore under its Campus for Research Excellence and Technological Enterprise (CREATE) program. The Disruptive & Sustainable Technology for Agricultural Precision (DiSTAP) is an interdisciplinary research group of the Singapore MIT Alliance for Research and Technology (SMART) Centre.

References

1. T. T. S. Lew, V. B. Koman, P. Gordiichuk, M. Park and M. S. Strano, The Emergence of Plant Nanobionics and Living Plants as Technology, *Advanced Materials Technologies*, 2020, **5**, 1900657.
2. T. T. S. Lew, R. Sarojam, I.-C. Jang, B. S. Park, N. I. Naqvi, M. H. Wong, G. P. Singh, R. J. Ram, O. Shoseyov, K. Saito, N.-H. Chua and M. S. Strano, Species-independent

analytical tools for next-generation agriculture, *Nature Plants*, 2020, **6**, 1408-1417.
3. V. B. Koman, T. T. S. Lew, M. H. Wong, S.-Y. Kwak, J. P. Giraldo and M. S. Strano, Persistent drought monitoring using a microfluidic-printed electro-mechanical sensor of stomata in planta, *Lab on a Chip*, 2017, **17**, 4015-4024.
4. T. T. S. Lew, V. B. Koman, K. S. Silmore, J. S. Seo, P. Gordiichuk, S.-Y. Kwak, M. Park, M. C.-Y. Ang, D. T. Khong, M. A. Lee, M. B. Chan-Park, N.-H. Chua and M. S. Strano, Real-time detection of wound-induced H2O2 signalling waves in plants with optical nanosensors, *Nature Plants*, 2020, **6**, 404-415.
5. J. P. Giraldo, M. P. Landry, S. M. Faltermeier, T. P. McNicholas, N. M. Iverson, A. A. Boghossian, N. F. Reuel, A. J. Hilmer, F. Sen, J. A. Brew and M. S. Strano, Plant nanobionics approach to augment photosynthesis and biochemical sensing, *Nature Materials*, 2014, **13**, 400-408.
6. S.-Y. Kwak, T. T. S. Lew, C. J. Sweeney, V. B. Koman, M. H. Wong, K. Bohmert-Tatarev, K. D. Snell, J. S. Seo, N.-H. Chua and M. S. Strano, Chloroplast-selective gene delivery and expression in planta using chitosan-complexed single-walled carbon nanotube carriers, *Nature Nanotechnology*, 2019, **14**, 447-455.
7. S.-Y. Kwak, J. P. Giraldo, M. H. Wong, V. B. Koman, T. T. S. Lew, J. Ell, M. C. Weidman, R. M. Sinclair, M. P. Landry, W. A. Tisdale and M. S. Strano, A Nanobionic Light-Emitting Plant, *Nano Letters*, 2017, **17**, 7951-7961.
8. P. Gordiichuk, S. Coleman, G. Zhang, M. Kuehne, T. T. S. Lew, M. Park, J. Cui, A. M. Brooks, K. Hudson, A. M. Graziano, D. J. M. Marshall, Z. Karsan, S. Kennedy and M. S. Strano, Augmenting the living plant mesophyll into a photonic capacitor, *Science Advances*, 2021, **7**, eabe9733.
9. M. H. Wong, J. P. Giraldo, S.-Y. Kwak, V. B. Koman, R. Sinclair, T. T. S. Lew, G. Bisker, P. Liu and M. S. Strano, Nitroaromatic detection and infrared communication from wild-type plants using plant nanobionics, *Nature Materials*, 2017, **16**, 264-272.
10. T. M. Klein, E. D. Wolf, R. Wu and J. C. Sanford, High-velocity microprojectiles for delivering nucleic acids into living cells, *Nature*, 1987, **327**, 70-73.
11. G. Demirer and M. Landry, Delivering genes to plants, *Chemical Engineering Progress*, 2017, **113**.
12. E. Neumann, M. Schaefer-Ridder, Y. Wang and P. H. Hofschneider, Gene transfer into mouse lyoma cells by electroporation in high electric fields, *The EMBO Journal*, 1982, **1**, 841-845.
13. Q. Chen and H. Lai, Gene Delivery into Plant Cells for Recombinant Protein Production, *BioMed Research International*, 2015, **2015**, 932161.
14. P. S. Vijayakumar, O. U. Abhilash, B. M. Khan and B. L. V. Prasad, Nanogold-Loaded Sharp-Edged Carbon Bullets as Plant-Gene Carriers, *Advanced Functional Materials*, 2010, **20**, 2416-2423.
15. J. Liu, F.-h. Wang, L.-l. Wang, S.-y. Xiao, C.-y. Tong, D.-y. Tang and X.-m. Liu, Preparation of fluorescence starch-nanoparticle and its application as plant transgenic vehicle, *Journal of Central South University of Technology*, 2008, **15**, 768-773.
16. F. Torney, B. G. Trewyn, V. S. Y. Lin and K. Wang, Mesoporous silica nanoparticles deliver DNA and chemicals into plants, *Nature Nanotechnology*, 2007, **2**, 295-300.
17. G. S. Demirer, H. Zhang, J. L. Matos, N. S. Goh, F. J. Cunningham, Y. Sung, R. Chang, A. J. Aditham, L. Chio, M.-J. Cho, B. Staskawicz and M. P. Landry, High aspect ratio nanomaterials enable delivery of functional genetic material without DNA integration in mature plants, *Nature Nanotechnology*, 2019, **14**, 456-464.
18. N. Mitter, E. A. Worrall, K. E. Robinson, P. Li, R. G. Jain, C. Taochy, S. J. Fletcher, B. J. Carroll, G. Q. Lu and Z. P. Xu, Clay nanosheets for topical delivery of RNAi for sustained protection against plant viruses, *Nature Plants*, 2017, **3**, 16207.
19. P. Hu, J. An, M. M. Faulkner, H. Wu, Z. Li, X. Tian and J. P. Giraldo, Nanoparticle Charge and Size Control Foliar Delivery Efficiency to Plant Cells and Organelles, *ACS Nano*, 2020, **14**, 7970-7986.
20. Y. Zhang, J. Yan, A. Avellan, X. Gao, K. Matyjaszewski, R. D. Tilton and G. V. Lowry, Temperature- and pH-Responsive Star Polymers as Nanocarriers with Potential for in Vivo Agrochemical Delivery, *ACS Nano*, 2020, **14**, 10954-10965.
21. P. J. Franks and G. D. Farquhar, The Effect of Exogenous Abscisic Acid on Stomatal Development, Stomatal Mechanics, and Leaf Gas Exchange in Tradescantia virginiana, *Plant Physiology*, 2001, **125**, 935-942.
22. Z. Sun, X. Jin, R. Albert and S. M. Assmann, Multi-level Modeling of Light-Induced Stomatal Opening Offers New Insights into Its Regulation by Drought, *PLOS Computational Biology*, 2014, **10**, e1003930.
23. S. SMITH, J. D. B. WEYERS and W. G. BERRY, Variation in stomatal characteristics over the lower surface of Commelina communis leaves, *Plant, Cell & Environment*, 1989, **12**, 653-659.
24. A. LAISK, V. OJA and K. KULL, Statistical Distribution of Stomatal Apertures of Vicia faba and Hordeum vulgare and the Spannungsphase of Stomatal Opening, *Journal of Experimental Botany*, 1980, **31**, 49-58.
25. I. Terashima, S.-C. Wong, C. B. Osmond and G. D. Farquhar, Characterisation of Non-Uniform Photosynthesis Induced by Abscisic Acid in Leaves Having Different Mesophyll Anatomies, *Plant and Cell Physiology*, 1988, **29**, 385-394.
26. K. A. Mott and T. N. Buckley, Patchy stomatal conductance: emergent collective behaviour of stomata, *Trends in Plant Science*, 2000, **5**, 258-262.
27. Y. Onoda, F. Schieving and N. P. R. Anten, A novel method of measuring leaf epidermis and mesophyll stiffness shows the ubiquitous nature of the sandwich structure of leaf laminas in broad-leaved angiosperm species, *Journal of Experimental Botany*, 2015, **66**, 2487-2499.
28. G. J. Jordan, R. J. Carpenter, A. Koutoulis, A. Price and T. J. Brodribb, Environmental adaptation in stomatal size independent of the effects of genome size, *New Phytologist*, 2015, **205**, 608-617.
29. H. KAISER, The relation between stomatal aperture and gas exchange under consideration of pore geometry and diffusional resistance in the mesophyll, *Plant, Cell & Environment*, 2009, **32**, 1091-1098.
30. L. T. Bertolino, R. S. Caine and J. E. Gray, Impact of Stomatal Density and Morphology on Water-Use Efficiency in a Changing World, *Frontiers in Plant Science*, 2019, **10**.
31. K. C. Fetter, S. Eberhardt, R. S. Barclay, S. Wing and S. R. Keller, StomataCounter: a neural network for automatic

stomata identification and counting, *New Phytol*, 2019, **223**, 1671-1681.

32. M. H. Wong, R. P. Misra, J. P. Giraldo, S.-Y. Kwak, Y. Son, M. P. Landry, J. W. Swan, D. Blankschtein and M. S. Strano, Lipid Exchange Envelope Penetration (LEEP) of Nanoparticles for Plant Engineering: A Universal Localization Mechanism, *Nano Letters*, 2016, **16**, 1161-1172.
33. R. L. Pinals, D. Yang, A. Lui, W. Cao and M. P. Landry, Corona Exchange Dynamics on Carbon Nanotubes by Multiplexed Fluorescence Monitoring, *Journal of the American Chemical Society*, 2020, **142**, 1254-1264.
34. T. T. S. Lew, M. H. Wong, S.-Y. Kwak, R. Sinclair, V. B. Koman and M. S. Strano, Rational Design Principles for the Transport and Subcellular Distribution of Nanomaterials into Plant Protoplasts, *Small*, 2018, **14**, 1802086.
35. T. T. S. Lew, M. Park, J. Cui and M. S. Strano, Plant Nanobionic Sensors for Arsenic Detection, *Advanced Materials*, 2021, **33**, 2005683.
36. M. Argos, T. Kalra, P. J. Rathouz, Y. Chen, B. Pierce, F. Parvez, T. Islam, A. Ahmed, M. Rakibuz-Zaman, R. Hasan, G. Sarwar, V. Slavkovich, A. van Geen, J. Graziano and H. Ahsan, Arsenic exposure from drinking water, and all-cause and chronic-disease mortalities in Bangladesh (HEALS): a prospective cohort study, *The Lancet*, 2010, **376**, 252-258.
37. K. S. Mohammed Abdul, S. S. Jayasinghe, E. P. S. Chandana, C. Jayasumana and P. M. C. S. De Silva, Arsenic and human health effects: A review, *Environmental Toxicology and Pharmacology*, 2015, **40**, 828-846.
38. G. Miller, K. Schlauch, R. Tam, D. Cortes, M. A. Torres, V. Shulaev, J. L. Dangl and R. Mittler, The Plant NADPH Oxidase RBOHD Mediates Rapid Systemic Signaling in Response to Diverse Stimuli, *Science Signaling*, 2009, **2**, ra45-ra45.